

Whole-brain mapping of behaviourally induced neural activation in mice

Dulcie A. Vousden · Jonathan Epp · Hiroyuki Okuno · Brian J. Nieman ·
Matthijs van Eede · Jun Dazai · Timothy Ragan · Haruhiko Bito ·
Paul W. Frankland · Jason P. Lerch · R. Mark Henkelman

Received: 29 November 2013 / Accepted: 3 April 2014
© Springer-Verlag Berlin Heidelberg 2014

Abstract The ability to visualize behaviourally evoked neural activity patterns across the rodent brain is essential for understanding the distributed brain networks mediating particular behaviours. However, current imaging methods are limited in their spatial resolution and/or ability to obtain brain-wide coverage of functional activity. Here, we describe a new automated method for obtaining cellular-level, whole-brain maps of behaviourally induced neural activity in the mouse. This method combines the use of transgenic immediate-early gene reporter mice to visualize neural activity; serial two-photon tomography to image the entire brain at cellular resolution; advanced image processing algorithms to count the activated neurons and align the datasets to the Allen Mouse Brain Atlas; and statistical analysis to identify the network of activated brain regions evoked by behaviour. We demonstrate the use of this approach to determine the whole-brain networks activated during the retrieval of fear

memories. Consistent with previous studies, we identified a large network of amygdalar, hippocampal, and neocortical brain regions implicated in fear memory retrieval. Our proposed methods can thus be used to map cellular networks involved in the expression of normal behaviours as well as to investigate in depth circuit dysfunction in mouse models of neurobiological disease.

Keywords Neuroimaging · Immediate-early genes · Memory · Functional networks · Serial two-photon tomography

Introduction

A key challenge in neuroscience is to understand the neural circuits that give rise to particular behaviours. Complex

D. A. Vousden (✉) · B. J. Nieman · M. van Eede · J. Dazai ·
J. P. Lerch · R. M. Henkelman
Mouse Imaging Centre, The Hospital for Sick Children,
25 Orde St., Toronto ON M5T 3H7, Canada
e-mail: d.vousden@utoronto.ca

D. A. Vousden · J. Epp · P. W. Frankland · J. P. Lerch
Program in Neuroscience and Mental Health, The Hospital for
Sick Children, 555 University Ave., Toronto ON M5G 1X8,
Canada

D. A. Vousden · B. J. Nieman · J. P. Lerch · R. M. Henkelman
Department of Medical Biophysics, University of Toronto,
Toronto, Canada

H. Okuno · H. Bito
Department of Neurochemistry, The University of Tokyo
Graduate School of Medicine, CREST-JST, Bunkyo-ku, Hongo,
113-0033 Tokyo, Japan
e-mail: hbito@m.u-tokyo.ac.jp

B. J. Nieman · R. M. Henkelman
Program in Physiology and Experimental Medicine,
The Hospital for Sick Children, Toronto, Canada

T. Ragan
TissueVision, Inc., 955 Massachusetts Ave Ste 316, Cambridge,
MA 02139, USA

P. W. Frankland
Institute of Medical Science, University of Toronto, Toronto,
Canada

P. W. Frankland
Department of Physiology, University of Toronto, Toronto,
Canada

behaviours, such as memory retrieval, depend on the coordinated activity of distributed networks of neurons across cortical and subcortical brain regions (Alivisatos et al. 2012; Guzowski et al. 2005). Understanding these networks therefore requires whole-brain approaches. The mouse is an excellent model for studying brain and behaviour relationships due to its physiological and genetic similarity to humans (Chinwalla et al. 2002), the ease with which its genome can be manipulated (Peters et al. 2007), and our ability to train mice to perform behavioural tasks relevant to human cognitive processes. Although techniques exist to assess neural activation in rodents at both macro- and micro-scopic levels, current methods are limited in their ability to do so at high resolution across the whole rodent brain. For instance, functional magnetic resonance imaging (fMRI) can obtain whole-brain coverage of neural activation patterns in vivo, but does so at a relatively coarse spatial resolution. Moreover, the types of behaviours that can be investigated with rodent fMRI are limited by the fact that the animal must be immobilized in the scanner and is therefore generally anaesthetized during imaging (Ferris et al. 2011). In vivo two-photon microscopy and electrophysiological recording, on the other hand, enable high-resolution visualization of neural activity; however, both techniques are very limited in their spatial coverage (Kerr and Denk 2008; Alivisatos et al. 2012). Thus, new imaging methods are needed to map the brain-wide neural circuits involved in the expression of behaviours, in a systematic and unbiased manner.

With this objective, we describe a novel method for automated, brain-wide mapping of behaviourally induced neural activation patterns in the mouse. Moving towards a functional connectomics requires the integration of several technologies. First, we need reliable reporters of neural activity evoked by particular behaviours or stimuli in freely behaving rodents. Transgenic mice expressing fluorescent reporters under immediate-early gene (IEG) promoters such as *c-fos* and *Arc/Arg3.1* have been used to visualize recent neural activity related to cognitive processes (Guzowski et al. 2005; Barth 2007; Okuno 2011; Shepherd and Bear 2011; Kawashima et al. 2013). Here, we used a transgenic *Arc-Venus* mouse line, which expresses the destabilized fluorescent Venus protein under the control of the activity-dependent *Arc* promoter (Kawashima et al. 2009; Okuno et al. 2012; Mikuni et al. 2013). Like other IEGs, *Arc* expression is induced by heightened synaptic activity and is believed to play a critical role in synaptic plasticity and memory consolidation and retrieval (Gusev et al. 2005; Tzingounis and Nicoll 2006; Okuno 2011; Shepherd and Bear 2011; Okuno et al. 2012; Yamasaki et al. 2012). Moreover, since resting-state levels of *Arc* expression are low, *Arc* induction is a reliable molecular readout of recent

neuronal activity induced by cognitive processes (Okuno 2011; Shepherd and Bear 2011).

Secondly, to visualize the neuronal activity reporter, we need methods for high-resolution, whole-brain imaging of brains. Here, we used a recently developed imaging tool, serial two-photon tomography (STPT), which combines two-photon microscopy with an integrated vibratome for sectioning and produces well-aligned, high-resolution 3D datasets (Ragan et al. 2012).

Finally, we need unbiased automated image-processing and analysis methods to identify and quantify areas of activity and to compare the resulting activity networks. Here, we used the open-source, automated cell segmentation tool CellProfiler to count fluorescently labelled neuronal cell bodies (Carpenter et al. 2006) and image registration algorithms (Lerch et al. 2011) to align the samples to the Allen Institute for Brain Science (AIBS) mouse brain reference atlas (Lein et al. 2007). This process enables us to quantify neuronal activation in each of the AIBS atlas' annotated regions and compare the activation patterns across subjects. Aligning the datasets to the AIBS atlas also ties the functional activation maps into a common coordinate space, allowing patterns of activity to be compared both with those evoked by other behaviours, and with maps of gene and protein expression.

The method presented here combines the use of transgenic mice that act as reports of neural activity, STPT, automated image processing algorithms, and statistical analysis (Fig. 1). We demonstrate the use of this method to identify the whole-brain neural activity patterns evoked by two well-characterized behaviours: retrieval of contextual and tone fear memories. In addition to mapping networks involved in the expression of normal behaviours, this is a powerful method to investigate network dysfunction in mouse models of neurobiological disease.

Materials and methods

Mice

Twenty-four homozygous transgenic male mice expressing destabilized Venus protein under control of the full-length *Arc* promoter (*Arc-Venus* mice) were used. Lines of transgenic mice harbouring the *Arc-pro-Venus-pest* transgene were generated in C57BL/6 by a procedure similar to that used to establish *Arc-pro-EGFP-Arc* transgenic mice (Okuno et al. 2012). Briefly, the *Venus* cDNA (Nagai et al. 2002) was subcloned into a plasmid containing the 7-kb regulatory region of the *Arc* gene (Kawashima et al. 2009). The Venus reporter was destabilized by adding a PEST signal sequence from the mouse ornithine decarboxylase with D433A/D434A mutations to accelerate its degradation

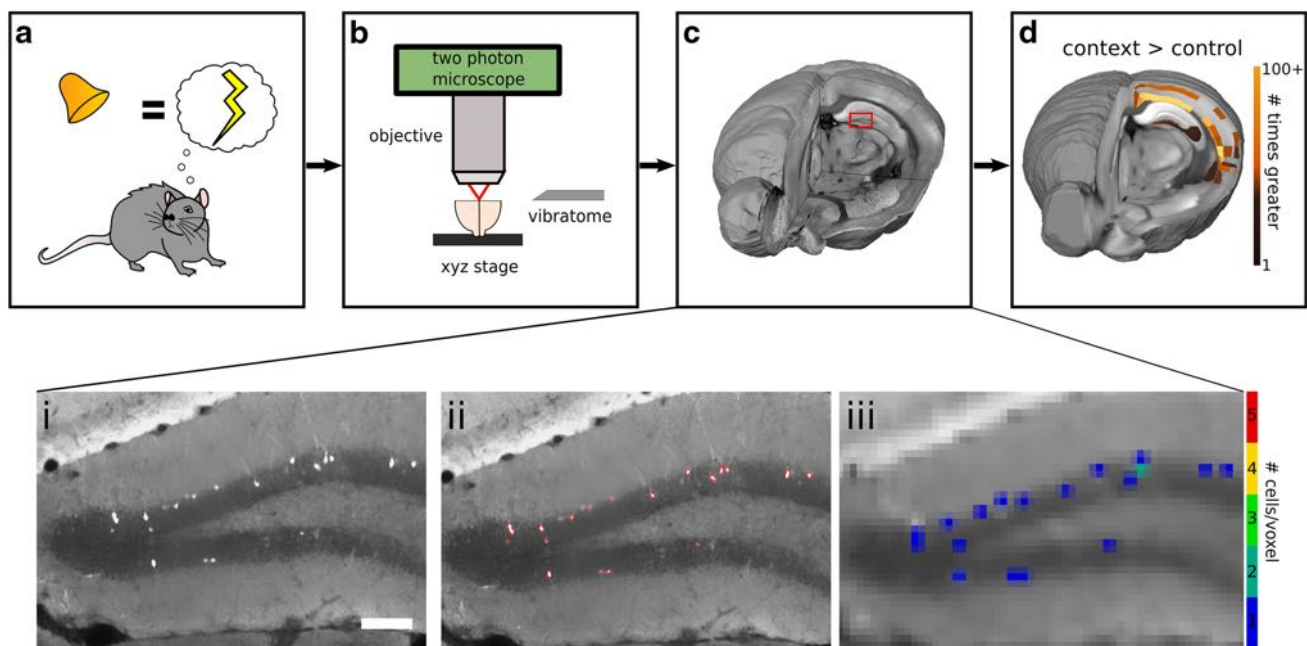


Fig. 1 Overview of the method. **a** Behavioural stimulation, such as fear memory retrieval, evokes neural activation and induces immediate-early genes (IEGs), such as *Arc*. Transgenic mice expressing fluorophores following IEG induction can be used to visualize recent neural activity. **b** Each brain sample is imaged as a series of coronal optical sections using serial two-photon tomography (STPT). STPT consists of a two-photon microscope and integrated vibratome and translation stages. **c** A 3D volume rendering of an *Arc-Venus* mouse brain imaged with STPT. An enlarged view of the region outlined in red is shown in

the bottom panels: **i** Visualization of fluorescently labelled neurons in the dentate gyrus using STPT. **ii** Automated cell segmentation software is used to identify fluorescent cell bodies in each coronal section. **iii** The samples and counts are stacked into 3D volumes and resampled at 25 μm isotropic resolution to obtain counts of the number of fluorescent neurons per 25 μm voxel. **d** Brain regions activated during recall of contextual fear memories: aligning the datasets to the Allen Mouse Brain Atlas enables statistical analysis to relate counts of number of activated neurons to retrieval of fear memories. Scale bar is 0.1 mm

rate (Li et al. 1998). The *Arc-pro-Venus-pest* transgene was microinjected into the pronucleus of fertilized mouse eggs. Detailed characterization of *Arc-pro-Venus-pest* transgenic mice will be described elsewhere (HO and HB, in preparation). Genomic integration of the transgene and reporter expression was analysed by PCR, southern blotting, western blotting and histological assays. Mice were housed in cages of 3–5, maintained on a 12-h light/dark cycle, and allowed ad libitum access to food and water. Mice were 8-week old when tested. All experiments were approved by the Animal Ethics Committee of the Hospital for Sick Children in Toronto and by Recombinant DNA and Animal Experiments Committees of the University of Tokyo Graduate School of Medicine. All mouse requests should be directed to Haruhiko Bito and Hiroyuki Okuno at the University of Tokyo.

Fear conditioning

Training

Prior to training, mice were handled for 2 min per day for 3 days. Mice were trained and tested in conditioning

chambers with stainless steel grid floors through which footshocks could be delivered. All 24 *Arc-Venus* mice were trained on a fear-conditioning task. During training, each mouse was placed individually in the training chamber. Two minutes later, it received five tone (2,800 Hz) and footshock pairings (30 s tone, which co-terminated with a 2 s shock, 0.5 mA) at 2 min intervals (Fig. 2a). Mice were returned to their homecage 1 min after the final footshock.

Testing

Forty-eight hours after training, memory recall was induced by exposing the mice to either the training context (Context, $n = 8$) or the tone cue in a novel context (Tone, $n = 8$), while a control group remained in their home cage during the retrieval session (Control, $n = 8$). The context group was placed in the training chamber without the tone cue, and freezing behaviour was assessed for 5 min (Fig. 2b). The tone group was placed in a novel, unfamiliar chamber, distinct from the training chamber, and presented with the training tone (2 min without tone followed by 3 min with tone) (Fig. 2b). Freezing behaviour was measured automatically (FreezeFrame, Actimetrics).

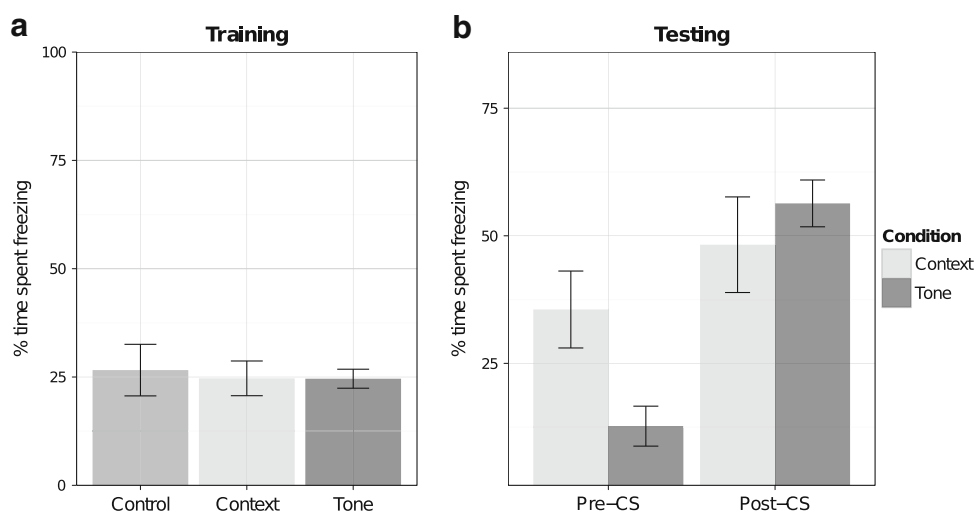


Fig. 2 Fear conditioning of Arc-Venus mice. **a** There was no difference in freezing in mice trained on the cued fear-conditioning paradigm. **b** Following presentation of the conditioned stimulus (CS) to the tone group, there was no difference in conditioned fear in mice recalling either contextual or tone fear memories (Post-CS). Pre-CS

refers to the time prior to tone presentation to the tone group, during which only the context group is exposed to their CS, the training environment, and exhibits a fear response. *Error bars* represent standard error of the mean

Sample preparation

The mouse brains were prepared for imaging as follows: three and a half hours following memory recall testing, the mice were anaesthetized by intraperitoneal (i.p.) injection of chloral hydrate and transcardially perfused with 50 mL of phosphate-buffered saline (PBS, pH 7.4, 25 °C) followed by 50 mL of cold 4 % formaldehyde. This time-point was chosen as it is the peak expression of the Venus fluorophore. The skulls were dissected and further fixed in 4 % formaldehyde at 4 °C for 24 h. The brains were then transferred to PBS and 0.02 % sodium azide at 4 °C before being embedded in 4 % agarose for imaging.

Imaging

We used serial two-photon tomography (STPT) to image the brains as datasets consisting of 200 coronal sections, evenly spaced by 75 μm with an in-plane resolution of 1.37 μm (Fig. 1b–c) (Ragan et al. 2012). STPT works as follows: the brain sample is glued to a microscope slide and mounted in a phosphate buffer bath on integrated xyz translation stages. Light (here 920 nm) from a Chameleon Ultra titanium-sapphire laser (coherent) passes through a tube and scan lens assembly toward a pair of scanning mirrors before being reflected by a short-pass dichroic toward a microscope objective (16 \times Nikon lens, 0.8 NA, WD 3.0 mm) (Ragan et al. 2012). The fluorescent signal from the sample is collected by the same objective, and then split by a dichroic mirror and directed onto two photomultiplier tubes (channel 1 and channel 2). After

optical imaging, an integrated vibratome mechanically sections the sample. Here, we used a 516-nm single-edge dichroic beamsplitter (Semrock FF516-di01-25 \times 36), which reduces background autofluorescence by splitting the light at 516 nm and collecting emitted light on two channels (channel 1: >516 nm, channel 2 <516 nm). Only channel 1 data were used for subsequent image processing and analysis.

Once the imaging parameters are set, the instrument software automatically controls scanning, stage motion, vibratome control, and data acquisition. The following sectioning parameters were specified: sectioning speed = 0.5 mm/s, blade vibration frequency = 60 Hz, cut velocity = 20 mm/s, delay = 8 s. For image acquisition, signal was collected from 40 μm below the sample surface, as a mosaic of 12 \times 8 overlapping tiles, each 832 \times 832 pixels. The xy stage movement was 900 μm and pixel size 1.37 μm . The total imaging time was approximately 9.5 h per sample. All imaging experiments and analyses were conducted blind to the experimental group of the mouse.

Image pre-processing

The individual tiles were saved as 16-bit tiff files. We used custom programs written in matlab and Python to process the data as follows: each tile was cropped by 15 pixels on each edge to remove illumination artefacts near the borders. Then to correct for uneven illumination, each tile was divided by the average-intensity image of all tiles in the sample. The illumination-corrected tiles were then stitched together into 2D coronal slices by computing the cross

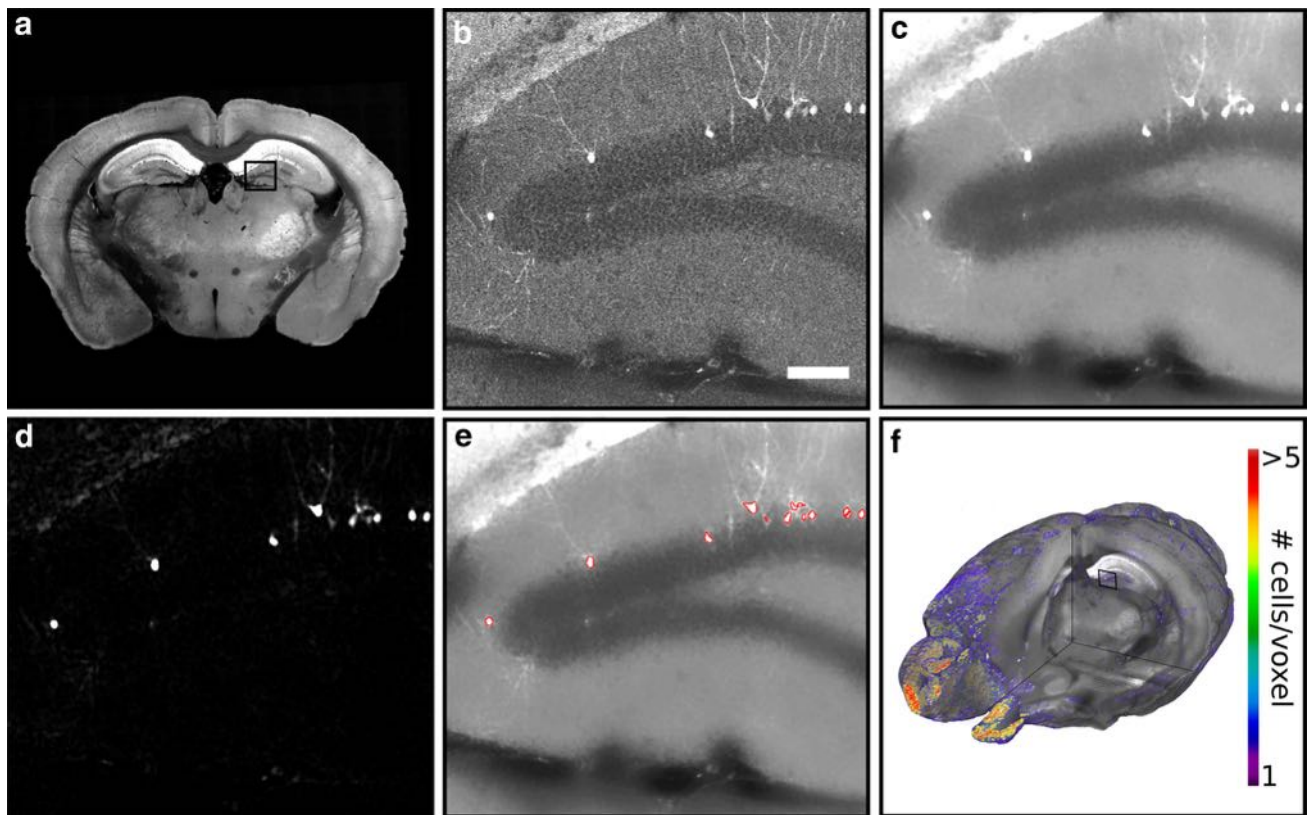


Fig. 3 Quantification of Arc-Venus+ neurons. Using the cell segmentation software CellProfiler, each 2D coronal image (a) in each brain sample was processed as follows: intensities were rescaled (b) and the image was blurred with small median and Gaussian bilateral filters (c) to reduce noise. Bright speckles were enhanced

(d) and used to identify cell bodies based on intensity and shape (e). The cell bodies in each 2D image were counted. Then, images and counts were stacked and resampled at 25 μm isotropic resolution to create 3D volumes of cell counts at each voxel (f). Scale bar represents 0.1 mm

correlation between tiles. At the overlapping regions, the pixels were blended using a weighted average of pixel intensities from contributing tiles.

Quantification of fluorescent neuronal cell bodies

To identify and localize Arc-Venus-labelled neurons that were activated during memory recall, we used the automated, open-source cell segmentation software CellProfiler to count fluorescent neuronal cell bodies in every 2D section of each sample (Figs. 1, 3) (Carpenter et al. 2006). A CellProfiler pipeline was created to identify neuronal cell bodies based on intensity, size, and shape. Each image was blurred to reduce noise, and then bright speckles of an appropriate size were enhanced to identify cell-body candidates. The cell bodies were then identified and filtered based on size, shape, and intensity, using a robust adaptive background filter. Finally, each identified object was reduced to one pixel and 25- μm blocks were used for cell counting. The sequential 2D optical sections acquired with STPT are inherently aligned (Ragan et al. 2012). We therefore used a custom python script to stack both the

smoothed 25- μm optical sections and separately, their corresponding counts, into 3-dimensional, 25- μm isotropic voxel datasets. This produces two 3D volumes for each brain: an anatomical volume and a volume of cell counts. For a full list of CellProfiler modules and parameters, see Appendix.

To ensure appropriate selection of CellProfiler parameters, the full dataset was divided into a training set and a validation set, each comprising half the samples from each group. The training set was used to tune the segmentation parameters listed above. Three sets of size, shape, and intensity filter parameter combinations were selected and used to process the training set. Once the optimal parameter set was found, the data were analysed as described below. The validation set was used to confirm the accuracy of this analysis. For the final analysis, the data were combined.

Image registration

To identify and compare the brain networks involved in recalling contextual and cued fear memories across all

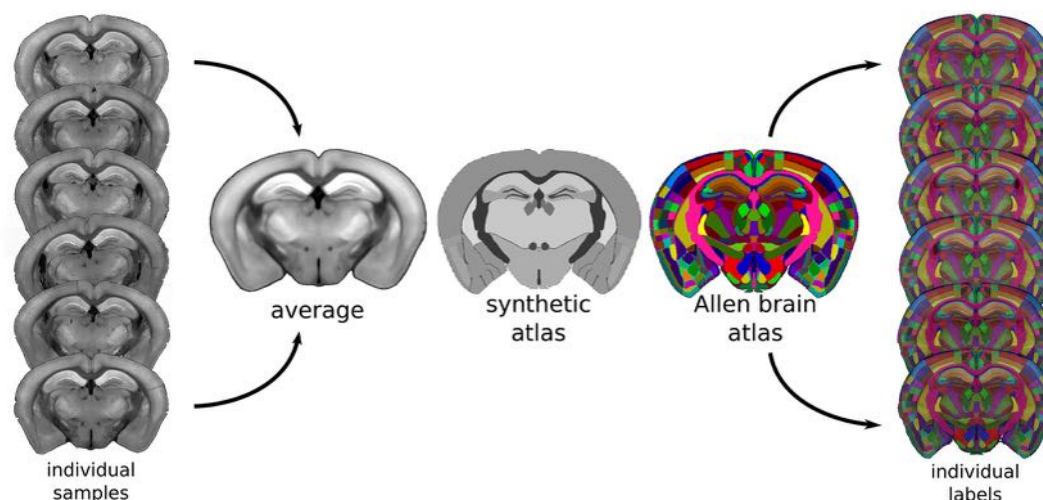


Fig. 4 Image registration process. The 3D serial two-photon tomography images and accompanying cell counts from all 24 mice were aligned to create an average of all brains in the study. This average was then aligned to the Allen Mouse Brain Atlas via a synthetic

subjects, all brains in the study were aligned using in-house image registration software (Fig. 4, for full details see Appendix) (Lerch et al. 2008, 2011; Kovacevic et al. 2005). Image registration finds a set of smooth transformations to align all brains in the study to a common coordinate system so that corresponding anatomical features are superimposed. Given the biased sampling acquired, with high in-plane resolution and 75- μm slice gaps, the datasets were resampled to isotropic 25 μm sampling using trilinear resampling for the images and nearest-neighbour resampling for the counts. Therefore, each downsampled voxel contained an estimate of the number of identified fluorescent cell bodies in that $25 \times 25 \times 25 \mu\text{m}^3$ voxel. Isotropic sampling allows the brain to be digitally resliced in any arbitrary direction, which is essential for aligning all the brains in the study into the same space for statistical comparisons between groups.

We used an automated intensity-based group-wise registration approach that first linearly aligns all images through a series of rotations, translations, scales, and shears, and then locally deforms each image through an iterative nonlinear process, bringing all brains into exact alignment (Lerch et al. 2008, 2011; Kovacevic et al. 2005) (Fig. 4, Appendix). Two iterations were used for the nonlinear stage. The registration was performed using in-house software based on the MNI autoreg tools, which use an elastic registration algorithm (Collins et al. 1994, 1995; Collins and Evans 1997). This process yields an average image of all brains in the study, as well as transforms that bring each individual image into exact alignment with this average (Fig. 4). These transforms were then applied to the corresponding datasets of cell counts so they too were

intermediate. Using these transforms, the Allen Mouse Brain Atlas annotations were backpropagated onto individual samples, enabling quantification of the number of cells in each segmented brain region. Full registration parameters are given in Appendix

aligned and could be compared. After resampling to 25 μm resolution, the STPT datasets were each ~ 400 MB in size. The registration of 24 samples took approximately 500 h of CPU time. However, this process is easily parallelizable, and here was run on a computing cluster. The registration process completes in approximately 10 h on a mid-sized cluster of 8 machines each with an 8-core processor. For a more detailed description of registration parameters for each stage see Appendix.

To localize fluorescence to particular brain regions we aligned the STPT average to the AIBS mouse brain reference atlas, which divides the brain into 670 annotated regions (Lein et al. 2007). This allows us to compute cell counts in each of the Allen Mouse Brain Reference Atlas' structures in each individual brain. The goal of image registration is to align homologous points or brain regions between samples; image registration is thus an ill-posed problem if these homologous points/regions do not exist or cannot be identified between samples. The Allen Mouse Brain Reference Atlas is Nissl stained, while the intensity of our Arc-Venus average depends on the pattern of Venus expression throughout the brain samples and on inherent variation in the amount of autofluorescence from different brain regions. As such, different brain regions are visible in the Arc-Venus and Allen Nissl samples, making precise registration difficult. To overcome this challenge, the STPT average was first aligned to an intermediate synthetic atlas of the whole brain that was in the same space as the Allen Mouse Brain Atlas. This atlas was created by merging structures in the Allen Mouse Brain Atlas annotations such that a similar set of structures as in the Arc-Venus average was visible (Fig. 4). Because our registration algorithms depend on computing the cross correlation between image

intensities, we then replaced the Allen Mouse Brain Atlas annotations with the corresponding structure's intensity in the STPT average (Fig. 4). This enabled precise alignment of the Arc-Venus average to the Allen Mouse Brain Atlas. The linear steps of the registration were performed using the MNI program register and in-house software using the autoreg tools described above, and the final nonlinear registration used a greedy symmetric diffeomorphic registration (the SyN algorithm in ANTS, Avants et al. 2008).

Statistical analysis

All analyses were performed using the R statistical software (version 2.15.3). For each structure in the Allen Mouse Brain Reference Atlas, a negative binomial regression model was used to determine whether there was an effect of testing group (Control, Context, or Tone) on the number of counted neurons. The incident rate ratio (IRR) is the ratio between one group and the reference group. For example, an IRR of 5 means that the expected count is five times greater in, for example, the context mice compared to the control animals. A negative binomial model was used because the count distributions did not follow a normal distribution, and the data were overdispersed (conditional mean < variance). Shapiro–Wilks tests were used to determine that the count distributions deviated significantly from normality.

To determine whether differences in mean intensity could be used to analyse group-wise differences in activation networks, we computed the mean fluorescence intensity in each structure segmented in the Allen Mouse Brain Atlas. To control for global differences in intensity, we also normalized the mean intensity in each structure in three separate ways: first, by dividing by the average intensity over the sample; and secondly, by dividing by the mean intensity in the corpus callosum or separately by the arbor vitae—white matter structures, in which we would expect no activation under any condition. A Shapiro–Wilks test was used to show that the intensities did not deviate significantly from normality. We therefore used a linear regression to determine whether there was an effect of testing condition on the mean intensity or on normalized mean intensity in each structure.

Negative binomial regression models were also used to test the relationship between the percentage of time spent freezing during testing and the number of counted neurons in each brain structure. For this analysis, only the tested mice (Context and Tone) were used. For all analyses, multiple comparisons were controlled for using the false-discovery rate at a 5 % threshold (Genovese et al. 2002). Throughout the text, q values will be used, which are p values adjusted for multiple testing using the FDR approach.

Results and discussion

Arc-Venus mice recalled different types of fear memories

Twenty-four Arc-Venus mice were trained on a fear-conditioning task in which they received five tone and shock pairings (Fig. 2a). Forty-eight hours after training, the mice were divided into three groups. Memory recall was induced by exposing the mice to either the training context (Context, $n = 8$) or the tone cue in a novel context (Tone, $n = 8$), while a control group remained in their home cage during the retrieval session (Control, $n = 8$) (Fig. 2b). Following presentation of the tone stimulus to the tone group, there was no difference in the conditioned freezing response between mice recalling contextual and tone memories (Fig. 2b, post-CS). Thus, although the mice were recalling different types of fear memories, the strength of the memory was the same between groups.

Brain-wide mapping of functional activation networks

To visualize Arc-Venus expression, we used serial two-photon tomography (STPT) to image the brains as 3D datasets of optical sections. We then used the automated cell segmentation software CellProfiler to count activated Arc-Venus-labelled neurons (Carpenter et al. 2006) and image registration to align all brains in the study along with their corresponding cell counts. This enabled us to compare the activation patterns across samples and to determine the brain networks involved in recalling contextual and tone fear memories.

Consistent with previous studies, we found that fear memory retrieval is associated with activation in a distributed network of brain areas, including regions of the hippocampus, amygdala, and neocortex (Fig. 5). Among the most significant results were the findings that compared to untested controls, mice recalling contextual fear memories showed significantly greater activation in the hippocampal formation (including dentate gyrus) (Maren 2001; Lee and Kesner 2004; Huff et al. 2006; Mamiya et al. 2009), lateral, medial, cortical amygdalar nuclei (Maren 2001; Ploski et al. 2008; Mamiya et al. 2009), subiculum, as well as visual (Frankland et al. 2004), ento- and ecto-rhinal (Corcoran et al. 2011; Tayler et al. 2013), retrosplenial (Corcoran et al. 2011), perirhinal (Campeau and Davis 1995; Corodimas and LeDoux 1995), and posterior parietal association areas of the cortex (Tayler et al. 2013) ($q < 0.05$ for all regions shown, Fig. 5). Similarly, compared to untested controls, mice recalling tone memories had significantly greater activation in the hippocampus (Mamiya et al. 2009), basolateral, lateral, medial, central, and cortical amygdalar nuclei (Ploski et al. 2008; Mamiya

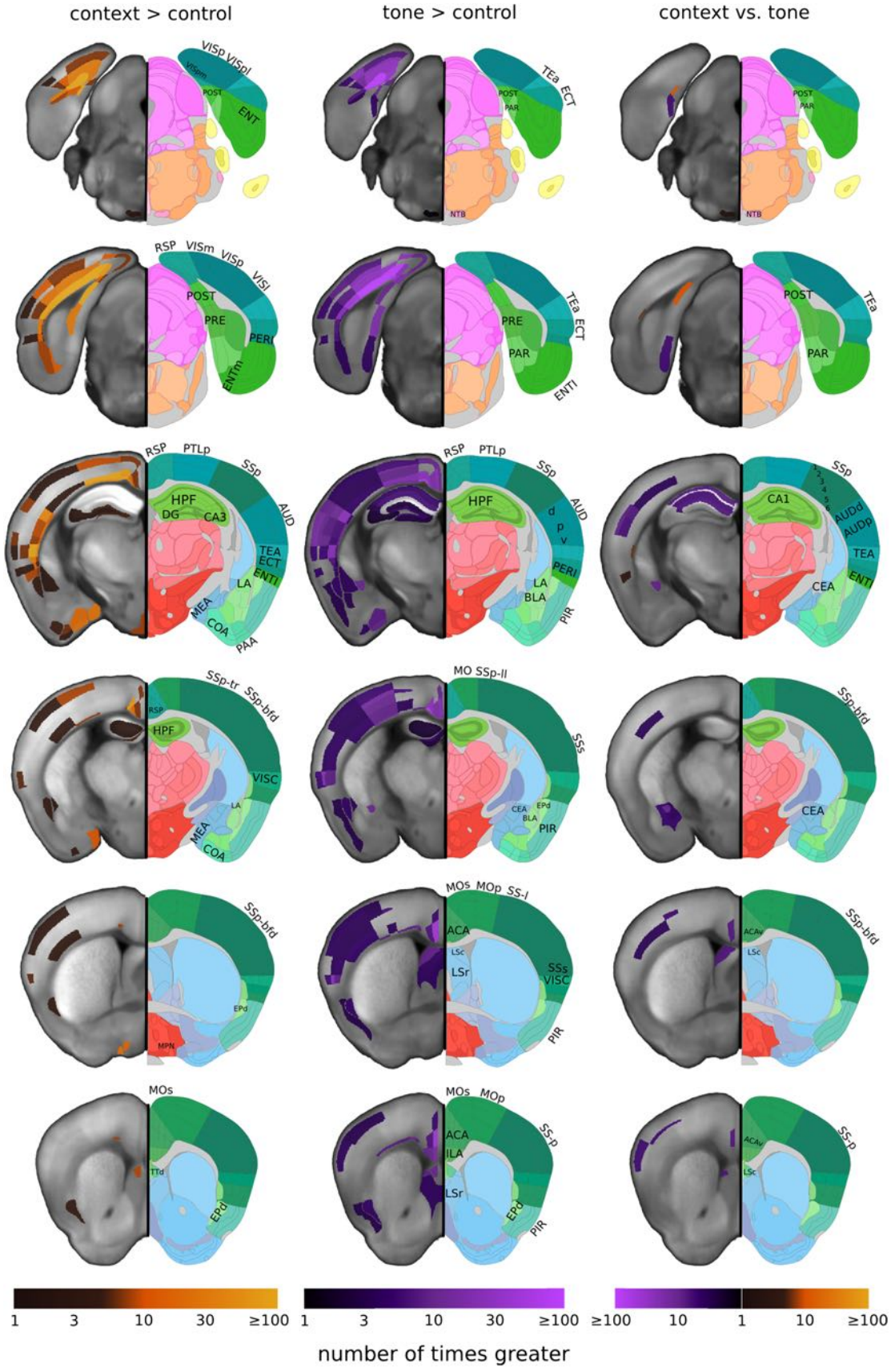


Fig. 5 Whole-brain networks involved in fear memory recall. (*Left*) Brain regions in which there were a significantly greater number of activated neurons in mice recalling contextual fear memories, compared to untested controls. (*Middle*) Regions where there were a significantly greater number of activated neurons in mice recalling tone fear memories compared to controls. (*Right*) Regions where there was a significant difference in the number of activated neurons in mice recalling contextual fear memories compared to tone memories (with colour indicating which showed more activated neurons). In all columns, the left half of the image shows individual labelled structures coloured according to the ratio of mean counts in one group compared to another, i.e. the fold increase of counts of activated neurons in one group relative to the reference group. The background image is the average of all brains in the study. The right half of the image shows the corresponding Allen Mouse Brain Atlas reference atlas annotations. For all coloured structures in the statistical maps (left hemisphere), there was a significant effect of testing group at a false-discovery rate (FDR) of 0.05. Allen Mouse Brain Atlas images obtained from the Allen Institute for Brain Science website: http://mouse.brain-map.org/experiment/thumbnails/100048576?image_type=atlas (Image numbers: 405, 382, 297, 261, 209, 169. Image credit: Allen Institute for Brain Science). Abbreviations: 1–6: Cortical layers 1–6; *ACA* anterior cingulate, *AUD* auditory (*d* dorsal, *p* primary, *v* ventral), *BLA* Basolateral amygdala, *CA1-3* Cornu ammonis 1-3, *CEA* Central amygdala, *COA* Cortical amygdala, *DG* dentate gyrus, *ECT* entorhinal, *ENT* Entorhinal area (*l* lateral, *m* medial), *Epd* endopiriform nucleus, *HPF* hippocampal formation, *ILA* infralimbic, *LA* Lateral amygdala, *LS* lateral septal nucleus (*r* rostral, *c* caudal), *MEA* medial amygdala, *MO* Motor area (*p* primary motor area, *s* secondary), *NTB* nucleus of the trapezoid body, *PAR* parasubiculum, *PERI* perirhinal, *PIR* piriform, *POST* postsubiculum, *PTLp* posterior parietal association, *PRE* presubiculum, *SS* Somatosensory area (*bfd* barrel field, *ll* lower limb, *p* primary, *s* supplemental, *tr* trunk), *TEA* temporal association, *Ttd* Taenia tecta, *RSP* retrosplenial, *VISC* visceral, *VIS* Visual area (*p* primary, *l* lateral *pl* posterolateral, *pm* posteromedial visual)

et al. 2009), and many cortical areas, including the auditory (LeDoux 2000), retrosplenial, somatosensory (Wei et al. 2002), and infralimbic cortices ($q < 0.05$ for all regions, Fig. 5).

While the contextual and tone memory networks were similar, we were also able to distinguish contextual fear memory networks from those involved in tone memory recall (Fig. 5). Compared to tone memory-recalling mice, mice recalling contextual memories showed significantly greater activation in the lateral areas of the entorhinal cortex, postsubiculum, and temporal association areas ($q < 0.05$ for all). In mice recalling tone memories, we found significantly greater activation in the auditory, somatosensory and anterior cingulate cortices, and subregions of the hippocampal formation and amygdala, compared to contextual memory-recalling mice ($q < 0.05$ for all, Fig. 5).

In addition to mapping the fold increase in counts onto the Allen Mouse Brain Atlas annotations, we also looked at the pattern of level of significance across the brain (Fig. 6). We found that the overall pattern in these mappings was very similar. Indeed, areas where there was a large fold

increase in neuronal activation in mice recalling either context or tone memories compared to controls were generally those with very small q values. Similarly, areas where there was a small fold increase in activation in memory-recalling animals compared to controls were generally those with larger q values.

Although the functional activation maps we obtained are largely an amalgam of regions previously reported in more targeted studies, we also saw significant activation in some less-expected brain regions. For instance, although the anterior cingulate (ACC) is typically implicated in more long-term fear memories (Frankland et al. 2004), we found a significant increase in Arc-Venus+ neurons in the mice recalling tone fear memories (Fig. 5). This is consistent, however, with reports that auditory fear memory retrieval induces a significant increase in the amount of cyclic-AMP responsive element-binding protein (CREB), a key transcription factor involved in memory formation and synaptic plasticity (Josselyn et al. 2001; Silva et al. 1998), in the ACC (Wei et al. 2002). Additionally, there was increased activation in the visual cortex of both groups of memory-recalling animals. This result may be due to increased Arc expression in visual areas following spatial exploration (Shepherd and Bear 2011). These results suggest that once a whole-brain functional activation map is obtained, further investigations (e.g. lesion studies or pharmacological/optogenetic interventions) may be beneficial to determine whether a particular brain region is strictly necessary for the expression of a behaviour of interest.

Quantification of neuronal activity in annotated brain regions

An advantage of this approach is its quantitative nature. Because the datasets were aligned to the AIBS mouse reference atlas, we were able to obtain counts of the number of activated neurons in each annotated region for each mouse. While this process was done automatically over each brain region, Fig. 6 shows the estimates of the number of activated Arc-Venus+ neurons in two areas of interest: the lateral amygdala and the granule cell layer of the dentate gyrus. There were five times as many activated neurons in the granule cell layer of the dentate gyrus in mice recalling both contextual (IRR = 5.19, $q \ll 0.0001$) and tone (IRR = 5.14, $q \ll 0.0001$) fear memories compared to untested controls (Fig. 7). Similarly, mice recalling contextual and tone fear memories had, respectively, three and four times as many activated neurons in the lateral amygdala as untested control mice (IRR = 3.16, $q = 0.03$ and IRR = 4.03, $q = 0.004$, respectively; Fig. 7). Thus, this method can be used to quantify the proportion of recently activated neurons in a particular

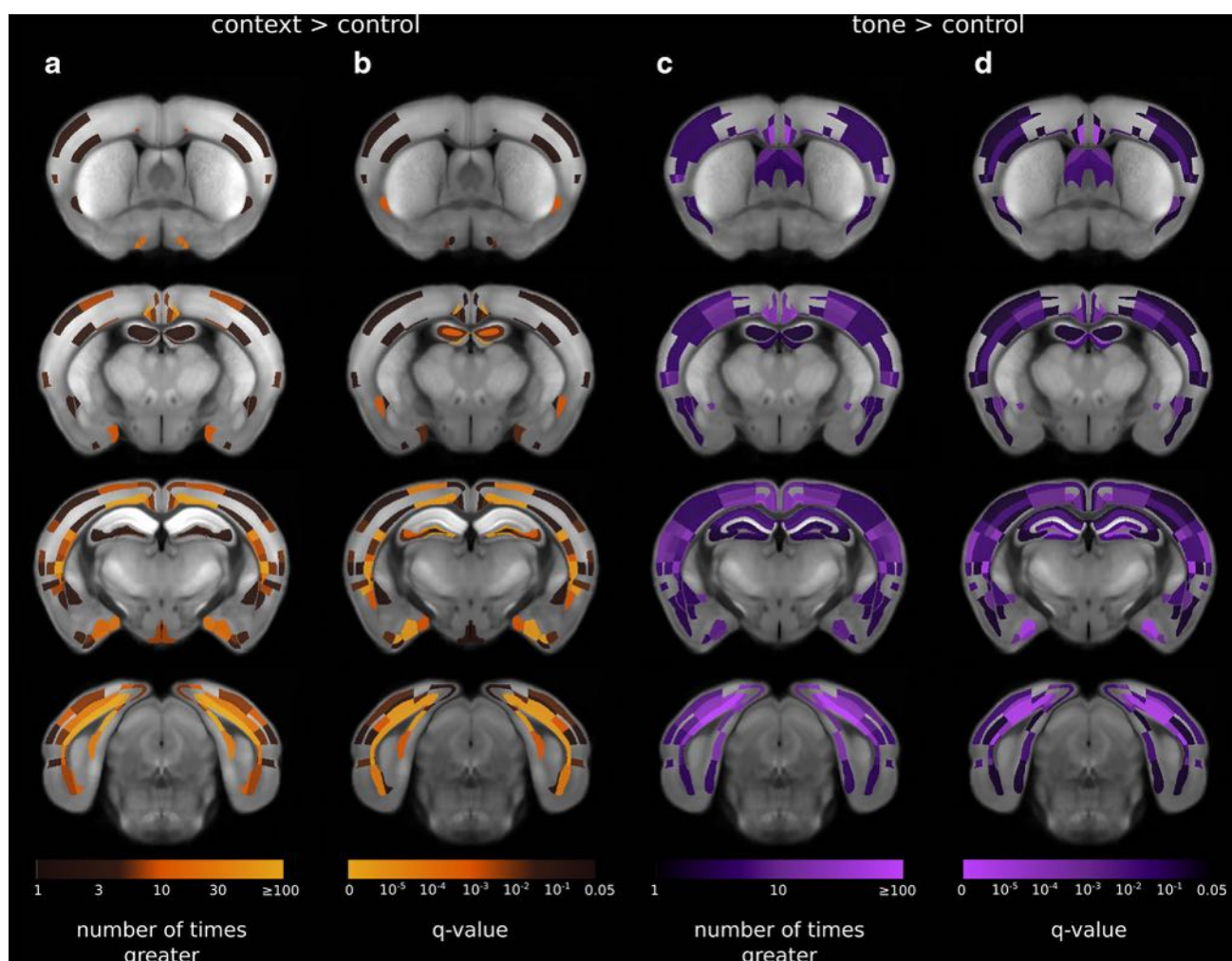


Fig. 6 Comparison of fold-increase and significance activation maps. Brain regions from Fig. 5 showing regions with a significantly greater number of activated neurons in mice recalling contextual (**a**) and tone (**c**) fear memories, compared to untested controls. Columns **b** and **d** show the same brain regions with the colour representing the

significance of the difference or q value (FDR-adjusted p values). Generally, the areas in which there was a greater increase in mice recalling context or tone fear memories were also those in which the differences were highly significant

brain region of interest, which could be useful in determining the size of the neuronal subpopulation needed to support a memory.

Effect of behaviour on neuronal activation

In fear-conditioning tasks, the amount of time the animal spends freezing during the recall test is commonly used as an indication of the strength of the animal's memory for the aversive event. With our approach, we obtain 3D volumes of counts of the number of recently active neurons in each defined brain region for each mouse. This approach therefore enables in-depth quantitative analyses of the relationship between the number of activated neurons in a given region and the mouse's behaviour during testing. We found several regions in which there was a significant

relationship between the percentage of time spent freezing during testing and the number of neurons in that region. For instance, in the posterior amygdalar nucleus, an area known to be critical for fear memory formation and retrieval (Ledoux 2000; Maren 2001), a greater amount of time freezing in the test was associated with a greater number of activated neurons (IRR = 1.02, $q = 0.037$) (Fig. 8a, b).

Conversely, in layer 6 of the posterolateral visual cortex, the extent of time freezing in the test was inversely correlated with the number of activated neurons in this region (IRR = 0.924, $q = 0.0005$) (Fig. 8c, d). One possible explanation for these seemingly opposing correlations in distinct areas is that mice that spend a greater amount of time freezing during testing may have formed a stronger association between the conditioned stimulus and

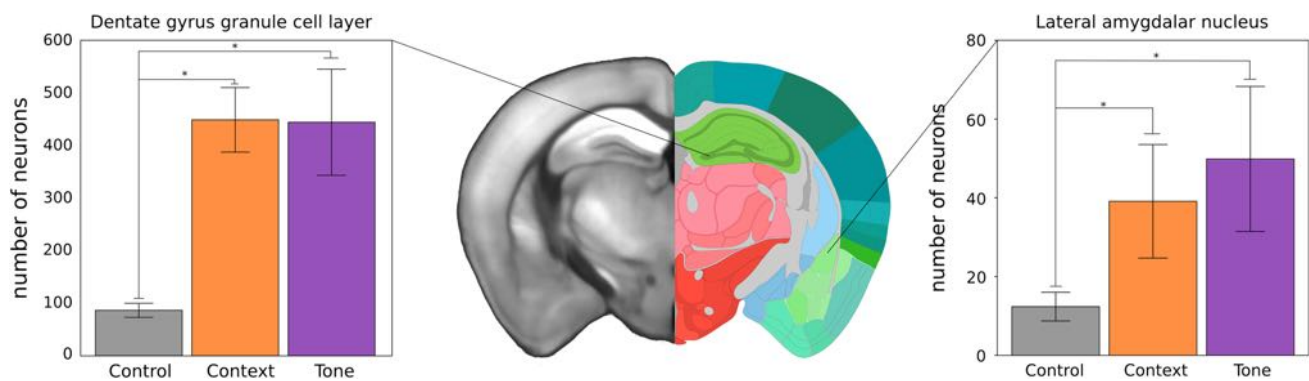


Fig. 7 Quantification of number of activated neurons across the brain. There was a significant increase in the number of activated neurons in the dentate gyrus of mice recalling contextual and tone fear memories compared to untested control animals (*left plot*, $q < 0.0001$, both). There was also a significant increase in number of activated neurons in the lateral amygdala in mice recalling contextual ($q = 0.03$) and tone ($q = 0.004$) fear memories, compared to controls (*right plot*). Error bars represent standard error of the

mean. In the brain image in the *middle*, the left half shows the average image of all brains in the study and the right half shows the Allen Mouse Brain Atlas reference atlas annotations (image 297). Allen Mouse Brain Atlas images obtained from the Allen Institute for Brain Science website: http://mouse.brain-map.org/experiment/thumbnails/100048576?image_type=atlas (Image credit: Allen Institute for Brain Science)

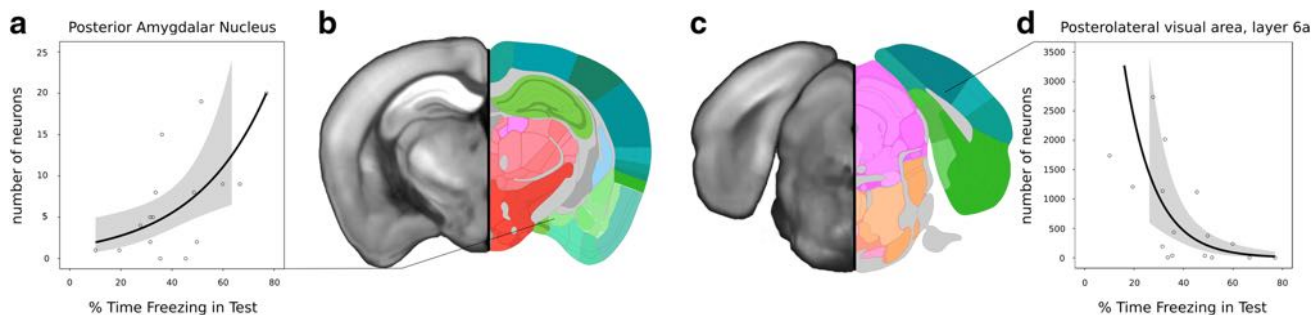


Fig. 8 Relationship between behaviour and neural activity. **a** Increased amount of time spent freezing during the memory recall test was associated with an increased number of activated Arc-Venus+ neurons in the posterior amygdala (negative binomial regression, $q = 0.037$). **b, c** Average of all samples acquired with serial two-photon tomography with Allen Mouse Brain Atlas reference atlas annotations overlaid to delineate the posterior amygdala and layer 6a of the posterolateral visual cortex. **d** Increased amount of time spent freezing during the memory recall

test was associated with a decreased number of activated Arc-Venus+ neurons in layer 6a of the posterolateral visual cortex ($q = 0.0005$). Dots represent individual samples. Fitted curve represents the predicted number of neurons in each brain area over the range of freezing percentages. Grey bands represent 95 % confidence intervals. Allen Mouse Brain Atlas images obtained from the Allen Institute for Brain Science website: http://mouse.brain-map.org/experiment/thumbnails/100048576?image_type=atlas (Image numbers: 309 and 388. Image credit: Allen Institute for Brain Science)

footshock, which may lead to an increased response in amygdalar nuclei and a subsequent stronger fear-mediated modulation of downstream structures. The increased freezing may thus perhaps gate and reduce neuronal activity in the visual cortical neurons involved in spatial exploration during fear retrieval. Alternatively, since IEG induction in the visual cortex has been shown to become stronger in response to a more novel/less familiar visual stimuli (Zhu et al. 1995), one may imagine that the mice which visually recognized less familiarity in the context (i.e. more novelty and hence more IEG expression in visual related systems) were the ones which showed comparably weaker freezing. Overall, the ability to quantitatively relate

individual differences in behaviour and neuronal activity patterns will enable future studies to more precisely probe the contribution of particular brain areas to behaviour.

Counting activated neurons is required as intensity measures are insufficient to dissociate functional activation networks

Obtaining the cellular-level resolution needed to extract neuronal counts from the data comes at the expense of long imaging times. We therefore asked whether this level of quantification is necessary to map differences in neural activation networks between testing conditions, or whether

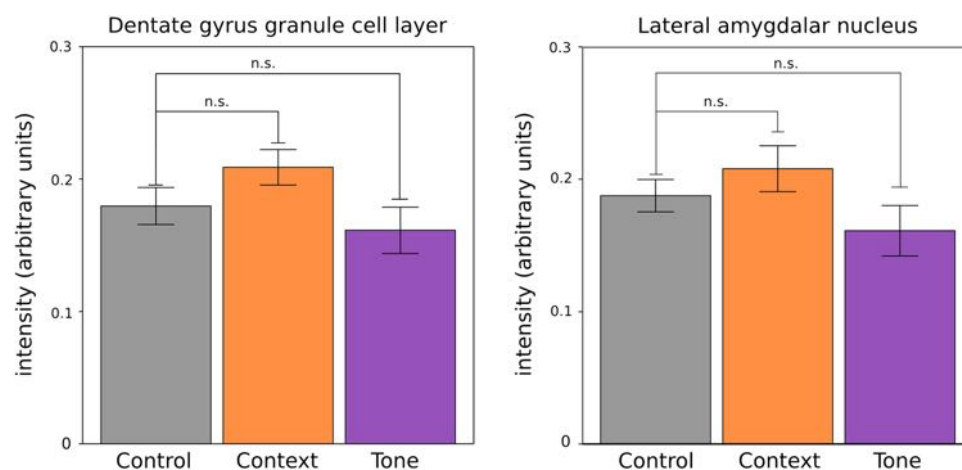


Fig. 9 Intensity-based methods are insufficient to dissociate activation networks. There was no difference in mean intensity in the dentate gyrus granule cell layer and lateral amygdala in mice recalling contextual and tone fear memories, compared to untested controls,

despite there being a significant difference in the number of activated neurons ($q > 0.05$, and see Fig. 5). There were no significant group-wise differences in intensity in any brain region, after multiple comparisons correction. *Error bars* are standard error of the mean

a coarser intensity-based analysis could suffice to dissociate the networks involved in recalling fear memories. There were no brain structures in which there was a significant effect of testing condition on the mean intensity of that structure, after correction for multiple comparisons, even if the false-discovery threshold was relaxed from 5 to 20 % (Fig. 9). There was also no significant effect of testing condition on the normalized mean intensity, when normalized by average intensity over the sample or by mean intensity in the corpus callosum or arbor vitae. Together, these results suggest that cognitively activated Arc-Venus+ neurons represent only a small number in most brain areas and are too scattered in space to be resolved using low-resolution, intensity-based approaches. These are clearly insufficient to distinguish the differences in Arc-Venus expression in mice recalling different types of fear memories, and thus cannot be used to determine functional activation networks evoked by memory recall.

Comparison with existing methodologies

To our knowledge, the imaging and image analysis workflow presented here is the first automated method able to identify and quantify behaviourally evoked neural activation across the whole mouse brain at single-neuron resolution. Compared to existing methods for identifying neural circuits involved in behaviour, this approach has several advantages. First, while *in vivo* two-photon fluorescence microscopy can be combined with calcium indicators or fluorescent reporters to image neural activity in the awake, behaving rodent, it is currently challenging to image large areas of the rodent cortex, and the depth achievable with *in vivo* imaging is limited by optical scattering (Kerr and

Denk 2008). Secondly, fluorescence microscopy or immunohistochemistry of mounted serial brain sections is very laborious to do across the whole-brain, and it is difficult to align the resulting 2D sections, which limits its use for whole-brain quantitative analyses at neuron-level resolution (Lein et al. 2007). Similarly, electrophysiological recordings of neural activity presently sample only sparse subsets of neurons within only a few brain regions (Alivisatos et al. 2012). Finally, though fMRI does acquire whole-brain activity patterns, it images at a much coarser spatial resolution, and the present requirement of anaesthesia restricts the types of behaviours that can be investigated (Ferris et al. 2011).

While the method described here overcomes these limitations, it is important to note that our automated approach is currently restricted to imaging fixed brain samples and thus does not permit *in vivo* imaging of neural activity in the freely behaving rodent, which limits the temporal resolution. However, we note that the use of transgenic or viral reporters of IEG expression is promising in this regard as well, as it allows the visualization of recent neural activation over the timescales of minutes to hours (Barth 2007; Eguchi and Yamaguchi 2009; Kawashima et al. 2009; Okuno et al. 2012). Additionally, while we used an Arc-Venus mouse line, this approach generalizes to any transgenic IEG reporter.

Considerations for future studies

While we investigated the brain networks activated in response to fear memory retrieval, in the future, this method could be used to determine the networks evoked by different stimuli or that are involved in the expression of

many other behaviours, including learning and memory formation in many domains (e.g. fear or spatial learning), object recognition, or social interaction. Additionally, this method could be used to investigate how functional activation networks are disrupted in mouse models of disease by crossing disease mouse models with immediate-early gene reporter mouse lines such as Arc-Venus or cfos-eGFP (Barth 2007; Reijmers et al. 2007). However, we note that any observed differences in functional activation networks between control and disease models may also be due to differences in synapse density. In such studies, it would therefore be important to control for this as much as possible, by comparing neural activation in wildtype animals and the model of interest in some sort of control activation task engaging the brain areas of interest, such as a tactile stimulation of the paw or visual stimulation.

Integration with the Allen Mouse Brain Atlas

Finally, although we aligned our dataset to the Allen Mouse Brain Atlas, the data can in principle be aligned to any atlas, provided the appropriate intermediate is created if necessary. For instance, the functional activation networks could be aligned to an MRI-based atlas or a mouse vascular atlas, enabling comparisons across imaging modalities. Additionally, the group-wise comparisons of neuronal activation can be performed voxel-wise, enabling the quantification of highly localized differences in activity. We note, however, that aligning the functional activation networks of different behaviours to the Allen Mouse Brain Atlas provides a standardized space for comparison. This enables the networks to be compared with maps of gene expression or cell types and will be particularly useful in comparing how activation networks are altered in models of disease.

Conclusion

In summary, we developed an automated method to detect neural activation patterns across the whole mouse brain. We used this method to obtain brain-wide maps of the areas involved in recalling different types of fear memories. Consistent with previous studies, we identified a large network of hippocampal, amygdala, and neocortical brain regions implicated in fear memory retrieval, which gives strong face validity to our approach. In the future, this method can be applied to identify the networks involved in less well-characterized behaviours, to understand how memory networks evolve with time, and to investigate how these neural circuits are disrupted in the pathogenesis and treatment of mouse models of complex brain disorders, such as Alzheimer's disease, schizophrenia, and autism

(Rudinskiy et al. 2012). In addition, this approach could be combined with graph-theoretical analyses to understand both healthy and disordered circuits from a network perspective (Bullmore and Sporns 2009; Wheeler et al. 2013). The combination of transgenic reporters of IEG expression, serial two-photon tomography (STPT) for high-resolution whole-brain imaging, and automated image registration and segmentation techniques provides a powerful means of mapping functional circuitry over the whole mouse brain.

Acknowledgments Research was supported by the Canadian Foundation for Innovation, Canadian Institute for Health Research (CIHR), Natural Science and Engineering Research Council (NSERC-DV), Ontario Research Foundation, a CREST-JST grant (HB and HO), and by Grants-in-Aid from JSPS (KIBAN to HO, WAKATE to HB) and from MHLW of Japan (to HB and HO). RMH was supported by a Canada Research Chair.

Conflict of interest TR is a shareholder and employee of Tissue-Vision, Inc.

Appendix: CellProfiler modules and parameters

The CellProfiler modules we used were as follows:

1. Rescale intensity: rescaled the image intensity range to be from 0 to 1 (Fig. 3b).
2. Smooth: blur each image with a small median filter (size = 3 pixels) and an edge-preserving bilateral Gaussian filter to reduce noise (Fig. 3c).
3. Enhance or suppress features: enhance bright speckles (size = 15 pixels) using a white tophat filter (Fig. 3d).
4. Identify primary objects: identify neuronal nuclei based on size (4–40 pixels), shape (threshold correction factor = 6), and intensity, using a robust adaptive background filter.
5. Measure object intensity and measure object size shape: measure the intensity and size of each identified object.
6. Filter objects: filtered objects based on intensity and shape (Fig. 3e).
7. Expand or shrink objects: reduce each identified object to one pixel for counting (Fig. 3f).

Image registration parameters

Aligning individual samples acquired with serial two-photon tomography (STPT) to achieve a consensus average

The registration was achieved using in-house software using the MNI autoreg tools (Collins et al. 1994; Kovacic et al. 2005; Collins and Evans 1997). First, all brains

were rigidly registered towards one of the samples in study. Then all possible pairwise 12-parameter registrations were performed to create a linear consensus average model of all the brains in the study. This linear average was used as the initial target for the final part of the registration. The individual images were locally deformed to this target using a multi-scale nonlinear alignment procedure using the Automatic Nonlinear Image Matching and Anatomical Labeling (ANIMAL) algorithm (Collins et al. 1997). This process was iterated a second time, using a finer resampling grid, with the resulting atlas used as the target for the second nonlinear stage.

Aligning average STPT image to Allen Mouse Brain Atlas

1. The STPT average and the synthetic intermediate atlas (in the same space as the Allen Mouse Brain Atlas) were first coarsely aligned manually with a 6 parameter registration using the MNI program register. Then the MNI autoreg tools (version 0.99.6) were used to align the two samples with a 12 parameter linear registration (3 shears, 3 scales, 3 translations, and 3 rotations (Kovacevic et al. 2005). We use the cross correlation of intensities for the linear optimization objective function with translation weights of 0.2 in each direction. The step size along each dimension was 1, and the simplex volume was 1.
2. The images were then aligned using nonlinear registration procedure using the Advanced Normalization Tools (ANTs) algorithm (Avants et al. 2008). We first blurred the images with a 0.05 mm fwhm Gaussian blurring kernel, and computed the gradients for each image. We used symmetric normalization, a diffeomorphic transformation model, using as similarity metrics a combination of cross correlation on the regular image intensities and cross correlation on the 3D gradient magnitudes. A Gaussian regularizer was used that operates both on the similarity metric and on the deformation field. The regularization blurring used a sigma of two for the gradient field and one for the deformation field. The gradient descent step size was 0.3. The radius for the similarity metric was three. At most 150 iterations were performed at each level.

References

- Avantis BB, Epstein CL, Grossman M, Gee JC (2008) Symmetric diffeomorphic image registration with cross-correlation: evaluating automated labeling of elderly and neurodegenerative brain. *Med Image Anal* 12:26–41
- Barth AL (2007) Visualizing circuits and systems using transgenic reporters of neural activity. *Curr Opin Neurobiol* 17:567–571
- Bullmore E, Sporns O (2009) Complex brain networks: graph theoretical analysis of structural and functional systems. *Nat Rev Neurosci* 10:186–198
- Campeau S, Davis M (1995) Involvement of subcortical and cortical afferents to the lateral nucleus of the amygdala in fear conditioning measured with fear-potentiated startle in rats trained concurrently with auditory and visual conditioned stimuli. *J Neurosci* 15:2312–2327
- Carpenter A, Jones T, Lamprecht M, Clarke C, Kang I, Friman O, Guertin D, Chang J, Lindquist R, Moffat J et al (2006) CellProfiler: image analysis software for identifying and quantifying cell phenotypes. *Genome Biol* 7:R100
- Chinwalla AT, Cook LL, Delehaunty KD, Fewell GA, Fulton LA, Fulton RS, Graves TA, Hillier LW, Mardis ER, McPherson JD et al (2002) Initial sequencing and comparative analysis of the mouse genome. *Nature* 420:520–562
- Collins DL, Evans C (1997) Animal: validation and applications of nonlinear registration-based segmentation. *Int J Pattern Recognit Artif Intell* 11:1271–1294
- Collins DL, Neelin P, Peters TM, Evans AC (1994) Automatic 3D intersubject registration of MR volumetric data in standardized Talairach space. *J Comput Assist Tomogr* 18:192–205
- Collins DL, Holmes CJ, Peters TM, Evans AC (1995) Automatic 3-D model-based neuroanatomical segmentation. *Hum Brain Mapp* 3:190–208
- Corcoran KA, Donnan MD, Tronson NC, Guzmán YF, Gao C, Jovasevic V, Guedeal AL, Radulovic J (2011) NMDA receptors in retrosplenial cortex are necessary for retrieval of recent and remote context fear memory. *J Neurosci* 31:11655–11659
- Corodimas KP, LeDoux JE (1995) Disruptive effects of posttraining perirhinal cortex lesions on conditioned fear: contributions of contextual cues. *Behav Neurosci* 109:613–619
- Eguchi M, Yamaguchi S (2009) In vivo and in vitro visualization of gene expression dynamics over extensive areas of the brain. *Neuroimage* 44:1274–1283
- Ferris CF, Smerkers B, Kulkarni P, Caffrey M, Afacan O, Toddes S, Stolberg T, Febo M (2011) Functional magnetic resonance imaging in awake animals. *Rev Neurosci* 22:665–674
- Frankland PW, Bontempi B, Talton LE, Kaczmarek L, Silva AJ (2004) The involvement of the anterior cingulate cortex in remote contextual fear memory. *Science* 304:881–883
- Genovese CR, Lazar NA, Nichols T (2002) Thresholding of statistical maps in functional neuroimaging using the false discovery rate. *Neuroimage* 15:870–878
- Gusev PA, Cui C, Alkon DL, Gubin AN (2005) Topography of Arc/Arg3.1 mRNA expression in the dorsal and ventral hippocampus induced by recent and remote spatial memory recall: dissociation of CA3 and CA1 activation. *J Neurosci* 25:9384–9397
- Guzowski JF, Timlin JA, Roysam B, McNaughton BL, Worley PF, Barnes CA (2005) Mapping behaviorally relevant neural circuits with immediate-early gene expression. *Curr Opin Neurobiol* 15:599–606
- Henkelman RM (2010) Systems biology through mouse imaging centers: experience and new directions. *Annu Rev Biomed Eng* 12:143–166
- Huff NC, Frank M, Wright-Hardesty K, Sprunger D, Matus-Amat P, Higgins E, Rudy JW (2006) Amygdala regulation of immediate-early gene expression in the hippocampus induced by contextual fear conditioning. *J Neurosci* 26:1616–1623
- Alivisatos AP, Chun M, Church GM, Greenspan RJ, Roukes ML, Yuste R (2012) The brain activity map project and the challenge of functional connectomics. *Neuron* 74:970–974

- Ji J, Maren S (2008) Lesions of the entorhinal cortex or fornix disrupt the context-dependence of fear extinction in rats. *Behav Brain Res* 194:201–206
- Josselyn SA, Shi C, Carlezon WA Jr, Neve RL, Nestler EJ, Davis M (2001) Long-term memory is facilitated by cAMP response element-binding protein overexpression in the amygdala. *J Neurosci* 21:2404–2412
- Kawashima T, Okuno H, Nonaka M, Adachi-Morishima A, Kyo N, Okamura M, Takemoto-Kimura S, Worley PF, Bito H (2009) Synaptic activity-responsive element in the Arc/Arg3.1 promoter essential for synapse-to-nucleus signaling in activated neurons. *Proc Natl Acad Sci USA* 106:316–321
- Kawashima T, Kitamura K, Suzuki K, Nonaka M, Kamijo S, Takemoto-Kimura S, Kano M, Okuno H, Ohki K, Bito H (2013) Functional labeling of neurons and their projections using the synthetic activity-dependent promoter E-SARE. *Nature Methods* 10:889–895
- Kerr JND, Denk W (2008) Imaging in vivo: watching the brain in action. *Nat Rev Neurosci* 9:195–205
- Kovacevic N, Henderson JT, Lifshitz N, Bishop J, Evans AC, Henkelman RM, Chen XJ (2005) A three-dimensional MRI atlas of the mouse brain with estimates of the average and variability. *Cereb Cortex* 15:639–645
- LeDoux JE (2000) Emotion circuits in the brain. *Annu Rev Neurosci* 23:155–184
- Lee I, Kesner RP (2004) Differential contributions of dorsal hippocampal subregions to memory acquisition and retrieval in contextual fear-conditioning. *Hippocampus* 14:301–310
- Lein ES, Hawrylycz MJ, Ao N, Ayres M, Bensinger A, Bernard A, Boe AF, Boguski MS, Brockway KS, Byrnes EJ et al (2007) Genome-wide atlas of gene expression in the adult mouse brain. *Nature* 445:168–176 and Website: 2012. Allen Institute for Brain Science. Allen Mouse Brain Atlas (Internet). Available from <http://mouse.brain-map.org/>
- Lerch JP, Carrol JB, Spring S, Bertram LN, Schwab C, Hayden MR, Henkelman RM (2008) Automated deformation analysis in the YAC128 Huntington disease mouse model. *NeuroImage* 39:32–39
- Lerch JP, Sled JG, Henkelman RM (2011) MRI phenotyping of genetically altered mice. *Methods Mol Biol* 711:349–361
- Li X, Zhao X, Fang Y, Jiang X, Duong T, Fan C, Huang CC, Kain SR (1998) Generation of destabilized green fluorescent protein as a transcription reporter. *J Biol Chem* 273:34970–34975
- Mamiya N, Fukushima H, Suzuki A, Matsuyama Z, Homma S, Frankland PW, Kida S (2009) Brain region-specific gene expression activation required for reconsolidation and extinction of contextual fear memory. *J Neurosci* 29:402–413
- Maren S (2001) Neurobiology of pavlovian fear conditioning. *Annu Rev Neurosci* 24:897–931
- Mikuni T, Uesaka N, Okuno H, Hirai H, Deisseroth K, Bito H, Kano M (2013) Arc/Arg3.1 is a postsynaptic mediator of activity-dependent synapse elimination in the developing cerebellum. *Neuron* 78:1024–1035
- Nagai T, Ibata K, Park ES, Kubota M, Mikoshiba K, Miyawaki A (2002) A variant of yellow fluorescent protein with fast and efficient maturation for cell-biological applications. *Nat Biotechnol* 20:87–90
- Okuno H (2011) Regulation and function of immediate-early genes in the brain: beyond neuronal activity markers. *Neurosci Res* 69:175–186
- Okuno H, Akashi K, Ishii Y, Yagishita-Kyo N, Suzuki K, Nonaka M, Kawashima T, Fujii H, Takemoto-Kimura S, Abe M et al (2012) Inverse synaptic tagging of inactive synapses via dynamic interaction of Arc/Arg3.1 with CaMKII β . *Cell* 149:886–898
- Peters LL, Robledo RF, Bult CJ, Churchill GA, Paigen BJ, Svenson KL (2007) The mouse as a model for human biology: a resource guide for complex trait analysis. *Nat Rev Genet* 8:58–69
- Ploski JE, Pierre VJ, Smucny J, Park K, Monsey MS, Overeem KA, Schafe GE (2008) The activity-regulated cytoskeletal-associated protein (Arc/Arg3.1) is required for memory consolidation of pavlovian fear conditioning in the lateral amygdala. *J Neurosci* 28:12383–12395
- Ragan T, Kadiri LR, Venkataraju KU, Bahlmann K, Sutin J, Taranda J, Arganda-Carreras I, Kim Y, Seung HS, Osten P (2012) Serial two-photon tomography for automated ex vivo mouse brain imaging. *Nat Methods* 9:255–258
- Reijmers LG, Perkins BL, Matsuo N, Mayford M (2007) Localization of a stable neural correlate of associative memory. *Science* 317:1230–1233
- Rudinskiy N, Hawkes JM, Betensky RA, Eguchi M, Yamaguchi S, Spires-Jones TL, Hyman BT (2012) Orchestrated experience-driven Arc responses are disrupted in a mouse model of Alzheimer's disease. *Nat Neurosci* 15:1422–1429
- Shepherd JD, Bear MF (2011) New views of Arc, a master regulator of synaptic plasticity. *Nat Neurosci* 14:279–284
- Silva AJ, Kogan JH, Frankland PW, Kida S (1998) Creb and memory. *Annu Rev Neurosci* 21:127–148
- Taylor KK, Tanaka KZ, Reijmers LG, Wiltgen BJ (2013) Reactivation of neural ensembles during the retrieval of recent and remote memory. *Curr Biol* 23:99–106
- Tzingounis AV, Nicoll RA (2006) Arc/Arg3.1: linking gene expression to synaptic plasticity and memory. *Neuron* 52:403–407
- Wei F, Qiu C-S, Liauw J, Robinson DA, Ho N, Chatila T, Zhuo M (2002) Calcium-calmodulin-dependent protein kinase IV is required for fear memory. *Nat Neurosci* 5:573–579
- Wheeler AL, Teixeira CM, Wang AH, Xiong X, Kovacevic N, Lerch JP, McIntosh AR, Parkinson J, Frankland PW (2013) Identification of a functional connectome for long-term fear memory in mice. *PLoS Comput Biol* 9:e1002853
- Yamasaki Y, Hashikawa K, Matsuki N, Nomura H (2012) Off-line Arc transcription in active ensembles during fear memory retrieval. *Eur J Neurosci*
- Zhu XO, Brown MW, McCabe BJ, Aggleton JP (1995) Effects of the novelty or familiarity of visual stimuli on the expression of the immediate early gene c-fos in rat brain. *Neuroscience* 69:821–829